Hindawi
International Journal of Aerospace Engineering
Volume 2018, Article ID 3968242, 10 pages
https://doi.org/10.1155/2018/3968242

Research Article

New Integrated Guidance and Control of Homing Missiles with an Impact Angle against a Ground Target

Shengjiang Yang,[1,2] Jianguo Guo,[1] and Jun Zhou[1]

[1]*Institute of Precision Guidance and Control, Northwestern Polytechnical University, Shaanxi 710072, China*
[2]*Beijing Aerospace Technology Institute, Beijing 100074, China*

Correspondence should be addressed to Jianguo Guo; guojianguo@nwpu.edu.cn

Received 4 February 2018; Revised 25 May 2018; Accepted 9 July 2018; Published 5 August 2018

Academic Editor: Giovanni Palmerini

A new integrated guidance and control (IGC) law is investigated for a homing missile with an impact angle against a ground target. Firstly, a control-oriented model with impact angle error of the IGC system in the pitch plane is formulated by linear coordinate transformation according to the motion kinematics and missile dynamics model. Secondly, an IGC law is proposed to satisfy the impact angle constraint and to improve the rapidity of the guidance and control system by combining the sliding mode control method and nonlinear extended disturbance observer technique. Thirdly, stability of the closed-loop guidance and control system is proven based on the Lyapunov stability theory, and the relationship between the accuracy of the impact angle and the estimate errors of nonlinear disturbances is derived from stability of the sliding mode. Finally, simulation results confirm that the proposed IGC law can improve the performance of the missile guidance and control system against a ground target.

1. Introduction

It is well known that the guidance and control system plays a key role in realizing the flight mission of missiles, and it becomes more and more important to improve the whole performance of the flight control system. The traditional guidance and control systems are separately designed based on the principle of separate frequency spectrum [1]. The effectiveness of the conventional design method has been confirmed in many engineering applications. However, it is argued that the design method may not fully exploit the synergistic relationships between these two interacting subsystems. As a result, the performance of the overall system may be constrained [2–4].

In order to improve the whole performance of the guidance and control system, an IGC method was proposed; that is, a whole model combining the guidance system and the autopilot system can be directly designed [5]. However, the increased dimension of the IGC model makes the controller design more difficult, and it is noted that the IGC model is a nonlinear model with mismatched uncertainties. Some control methods, such as the sliding mode control [6], adaptive control [7], and θ-D method [8], have been employed to design the IGC law in recent literatures. In general, IGC methods could be classified into the following two categories.

The first category method mainly focuses on the two-loop control structure in an IGC framework, and the outer loop and inner loop are separated in the guidance and control system [9–12] due to inherent time scale separation between the faster and slower dynamics. Although the outer loop takes the body rates as the virtual control input to directly yield the body rate command and the inner loop tracks the body rate commands with fin deflections as the control inputs, the settling time of response of different loops affects the performance of the whole system due to the delay problem. In fact, the first method is similar to the traditional design method of the guidance and control system.

The second category method for the IGC system combines the backstepping technique and the other control methods [13–19], such as the small-gain method [14], input-to-state stability theory [15], and dynamic surface

control technique [16–19]. The model of the IGC system can be written as a strict feedback system under reasonable assumptions, and some virtual control inputs can be obtained by the backstepping technique [19]. However, the filters/differentiators have to be utilized to overcome the calculating expansion problem caused by analytic differentiation of virtual control inputs. The rapidity of the IGC system decreases because the delay time increases by introducing the filters/differentiators.

In order to overcome the delay problem, a new IGC law is presented for a homing missile with an impact angle against a ground target, motivated by the sliding surface technique consisting of the system states and the estimated states [20, 21] derived from the nonlinear disturbance observers.

The contributions of this paper lie in the following aspects.

(a) A new control-oriented model with impact angle error of the IGC system in the pitch plane is built by combining the missile dynamics model and motion kinematics between the missile and target.

(b) A novel IGC law is proposed for a homing missile to satisfy the impact angle constraint and to improve rapidity of the IGC system by using the sliding mode control and the nonlinear disturbance observer technique.

(c) The stability of the closed-loop system is proven by using the Lyapunov stability theory, and the relationship between the accuracy of the impact angle and the estimate error of nonlinear disturbances is derived from the stability of the sliding mode.

(d) The proposed IGC law is evaluated by comparison with the classic guidance and control law and the other IGC law for a homing missile with an impact angle against a ground target.

The rest of this paper is organized as follows: in Section 2, the control-oriented model of the IGC system for the missile is established by linear coordinate transformation. A new IGC law is presented and the stability of the closed-loop system is proven in Section 3. Finally, the numerical simulation results are provided in Section 4, and conclusions are reported in Section 5.

2. Control-Oriented Dynamics Model

2.1. Nonlinear Motion Kinematics. The two-dimensional engagement dynamics model is described in Figure 1.

$$R\dot{q} = V_M \sin(q-\theta) + V_{T1}, \tag{1}$$

$$\dot{R} = -V_M \cos(q-\theta) + V_{T2}, \tag{2}$$

$$V_M\dot{\theta} = n_{yM} - g\cos\theta, \tag{3}$$

where q is the line-of-sight (LOS) angle and R, θ, V_M, and n_{yM} are the relative distance, the flight path angle, the velocity, and the acceleration of the missile, respectively.

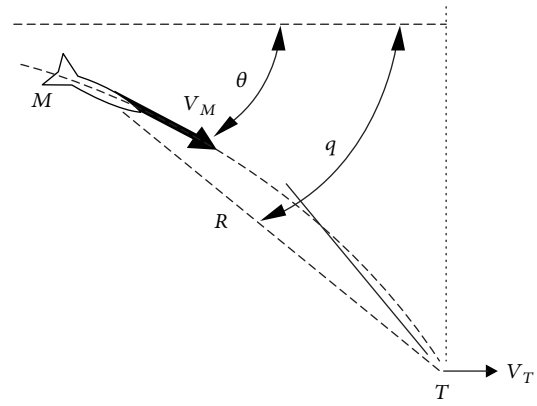

Figure 1: Two-dimensional engagement geometry.

V_{T1} and V_{T2} are unknown velocities with respect to the maneuver target on the ground, and g is acceleration of gravity.

By differentiating (1), and substituting (1), (2), and (3) into the derivative, it is easy to obtain

$$\ddot{q} = a_{11}\dot{q} + a_{12}n_{yM} + \Delta_q, \tag{4}$$

where $a_{11} = \dot{V}_M/V_M - 2\dot{R}/R$, $a_{12} = -\dot{R}/RV_M$, and $\Delta_q = -(\dot{V}_M/RV_M)V_{T1} + \dot{V}_{T1}/R + (V_{T2}/RV_M)n_{yM} - ((-\dot{R}+V_{T2})/RV_M)g\cos\theta$ are unknown uncertainties due to maneuver targets on the ground.

2.2. Missile Dynamics Model in the Pitch Plane. The longitude model of a missile in the pitch plane is described as [22]

$$\dot{\alpha} = w_z - \frac{57.3QSc_y^{\alpha} + P}{mV_m}\alpha + \Delta_{\alpha},$$

$$\dot{w}_z = \frac{QSL^2 m_z^{\bar{w}_z}}{J_z V_m} w_z + \frac{57.3QSLm_z^{\alpha}}{J_z V_m}\alpha + \frac{57.3QSLm_z^{\delta_z}}{J_z}\delta_z + \Delta_w, \tag{5}$$

where α is the angle of attack, w_z is the angular pitch rate, δ_z is the deflection angle for pitch control, m is the missile mass, Q is the dynamic pressure, S is the aerodynamic reference area, L is the reference length, P is the thrust of the missile, J_z is the moment of the inertia about z-axis, c_y^{α} is the lift force derivative with respect to the attack angle, and m_z^{α}, $m_z^{\bar{w}_z}$, and $m_z^{\delta_z}$ represent the pitch moment derivatives with respect to the attack angle, the nondimensional angular pitch rate, and the deflection angle for pitch control, respectively. Δ_{α} and Δ_w are unknown-bounded uncertainties of the missile-related parameters [22], for example, the aerodynamic coefficients.

2.3. Control-Oriented Model of the IGC System. The control-oriented model of the IGC system is built to design the IGC law. Assuming that q_M is the desired impact LOS

angle at the engagement time, the following equation and inequality hold:

$$R\dot{q} = V_M \sin(q-\theta) + V_{T1} = 0, \quad |q_M - \theta_M| < \frac{\pi}{2}, \tag{6}$$

where θ_M is the desired impact flight path angle at the engagement time.

Noting that $V_M \gg V_{T1}$, it is easy to obtain

$$q_M \approx \theta_M. \tag{7}$$

Let

$$e_q = q - q_M \approx q - \theta_M. \tag{8}$$

Differentiation (8) yields

$$\dot{e}_q = \dot{q}. \tag{9}$$

The acceleration of the missile is described as

$$n_{yM} = \frac{57.3QSc_y^{\alpha} + P}{m}\alpha + \Delta n_{yM}, \tag{10}$$

where Δn_{yM} is the unknown-bounded uncertainty of the missile-related parameters [23].

It is obtained from (4), (8), and (9) that

$$\ddot{e}_q = \ddot{q} = a_{11}\dot{q} + a_{13}\alpha + \Delta_e, \tag{11}$$

where $a_{13} = ((57.3QSc_y^{\alpha} + P)/m)a_{12}$ and $\Delta_e = a_{12}\Delta n_{yM} + \Delta_q$ are unknown uncertainties due to Δn_{yM} and Δ_q.

According to the above analysis, the control-oriented model of the IGC system for a homing missile against a ground target in the pitch plane can be described as

$$\dot{x}_1 = x_2, \tag{12}$$

$$\dot{x}_2 = x_3 + d_2, \tag{13}$$

$$\dot{x}_3 = x_4 + d_3, \tag{14}$$

$$\dot{x}_4 = a_{14}x_3 + a_{15}x_4 + bu + d_4, \tag{15}$$

where $x_1 = e_q$, $x_2 = \dot{e}_q$, $x_3 = a_{13}\alpha$, $x_4 = a_{13}w_z$, $u = \delta_z$, $a_{14} = 57.3QSLm_z^{\alpha}/J_zV_m a_{13}$, $a_{15} = QSL^2m_z^{\bar{w}_z}/J_zV_m a_{13}$, $b = (57.3QSLm_z^{\delta_z}/J_z)a_{13}$, $d_2 = a_{11}\dot{q} + \Delta_e$, $d_3 = -((57.3QSc_y^{\alpha} + P)/mV_m)a_{13}\alpha + a_{13}\Delta_{\alpha}$, and $d_4 = a_{13}\Delta_w$.

Remark 1. a_{12}, a_{13}, a_{14}, a_{15}, and b are known constants due to aerodynamic data. According to the definitions of the disturbance d_i $(i = 2, 3, 4)$ in the models (12), (13), (14), and (15), from a practical point of view, they represent the uncertainties coming from the missile-target motion kinematics and aerodynamic forces and moments of the missile.

Assumption 1. The disturbance d_i $(i = 2, 3, 4)$ and the first-order derivative of d_2 in the systems (12), (13), (14), and (15) are assumed to be bounded by known constants.

3. Control Design and Stability Analysis

Note that the control-oriented model of the IGC system for a homing missile is affected by the mismatched uncertainties; a new sliding mode controller is designed for the IGC system to exploit the synergistic relationship between guidance and autopilot subsystems. Meanwhile, the mismatched disturbances in the control-oriented model are estimated by using the nonlinear disturbance observer to compensate the sliding mode controller.

3.1. New IGC Law Design. Considering the control-oriented models (12), (13), (14), and (15) of the IGC system, a sliding surface with disturbance estimates is chosen as

$$s = c_1x_1 + c_2x_2 + c_3x_3 + x_4 + \hat{\dot{d}}_2 + c_3\hat{d}_2 + \hat{d}_3, \tag{16}$$

where $c_1 > 0$, $c_2 > 0$, and $c_3 > 0$ are chosen to satisfy the Hurwitz polynomial $g(\lambda) = c_1 + c_2\lambda + c_3\lambda^2 + \lambda^3$. $\hat{\dot{d}}_2$, $\hat{d}_2$, and $\hat{d}_3$ are the estimates of $\dot{d}_2$, d_2, and d_3, respectively.

In order to obtain the abovementioned estimates, three nonlinear disturbance observers based on [24] for the IGC models (12), (13), (14), and (15) are designed as follows:

$$\hat{d}_2 = p_{21} + l_{21}x_2, \tag{17}$$

$$\dot{p}_{21} = -l_{21}\left(x_3 + \hat{d}_2\right) + \hat{\dot{d}}_2, \tag{18}$$

$$\hat{\dot{d}}_2 = p_{22} + l_{22}x_2, \tag{19}$$

$$\dot{p}_{22} = -l_{22}\left(x_3 + \hat{d}_2\right), \tag{20}$$

$$\hat{d}_3 = p_{31} + l_{31}x_3, \tag{21}$$

$$\dot{p}_{31} = -l_{31}\left(x_4 + \hat{d}_3\right), \tag{22}$$

$$\hat{d}_4 = p_{41} + l_{h41}x_4, \tag{23}$$

$$\dot{p}_{41} = -l_{41}\left(a_{14}x_3 + a_{15}x_4 + bu + \hat{d}_4\right), \tag{24}$$

where p_{21}, p_{22}, p_{31}, and p_{41} are auxiliary variables and l_{21}, l_{22}, l_{31}, and l_{41} are the elements of the positive observer gain matrix to be designed.

The estimate errors are also defined as $\tilde{e}_{d2} = [\tilde{d}_2, \tilde{\dot{d}}_2]$, $\tilde{e}_{d3} = \tilde{d}_3$, and $\tilde{e}_{d4} = \tilde{d}_4$ where $\tilde{d}_2 = d_2 - \hat{d}_2$, $\tilde{\dot{d}}_2 = \dot{d}_2 - \hat{\dot{d}}_2$, $\tilde{d}_{3h} = d_{3h} - \hat{d}_{3h}$, and $\tilde{d}_3 = d_3 - \hat{d}_3$. It is also obtained from [24] that $\|\tilde{e}_{d2}\| \le \lambda_2$, $|\tilde{e}_{d3}| \le \lambda_3$, and $|\tilde{e}_{d4}| \le \lambda_4$, where $\lambda_i > 0$, for $i = 2, 3, 4$. It is easily obtained as

$$\left|\tilde{d}_2\right| \le \lambda_2, \quad \left|\tilde{\dot{d}}_2\right| \le \lambda_2, \quad \left|\tilde{d}_3\right| \le \lambda_3, \quad \left|\tilde{d}_4\right| \le \lambda_4. \tag{25}$$

Meanwhile, it can be also obtained from the disturbance observers (17), (18), (19), (20), (21), (22), (23), and (24) that

$$\dot{\tilde{d}}_2 = \dot{p}_{22} + \dot{l}_{22}x_2 = l_{22}\left(d_2 - \hat{d}_2\right) = l_{22}\tilde{d}_2, \tag{26}$$

$$\dot{\tilde{d}}_2 - \dot{\hat{d}}_2 = \dot{p}_{21} + l_{21}\dot{x}_2 - \dot{\hat{d}}_2 = l_{21}\left(d_2 - \hat{d}_2\right) = l_{21}\tilde{d}_2, \tag{27}$$

$$\dot{\tilde{d}}_3 = \dot{p}_{31} + l_{31}\dot{x}_3 = l_{31}\left(d_3 - \hat{d}_3\right) = l_{31}\tilde{d}_3. \tag{28}$$

Computing the derivative of $\dot{s}$ along systems (12), (13), (14), and (15), it can be obtained as

$$\begin{aligned} s = {} & c_1x_2 + c_2(x_3 + d_2) + c_3(x_4 + d_3) + a_{14}x_3 + a_{15}x_4 + bu \\ & + d_4 + \dot{\tilde{d}}_2 + c_3\dot{\tilde{d}}_2 + \dot{\tilde{d}}_3. \end{aligned} \tag{29}$$

Accordingly, the new sliding controller for the control-oriented models (12), (13), (14), and (15) is obtained as

$$\begin{aligned} u = -\frac{1}{b}\Big[& c_1x_2 + c_2x_3 + c_3x_4 + a_{14}x_3 + a_{15}x_4 + c_2\dot{\hat{d}}_2 + c_3\dot{\hat{d}}_2 \\ & + c_3\hat{d}_3 + \hat{d}_4 + k_hs + \varepsilon_h \operatorname{sgn}(s)\Big], \end{aligned} \tag{30}$$

where $k > 0$ and $\varepsilon > \eta = (c_2 + l_{22} + c_3l_{21})\lambda_2 + (c_3 + l_{31})\lambda_3 + \lambda_4$.

3.2. Stability Analysis. In order to illustrate the effectiveness of the proposed IGC, the stability of a closed system is analyzed as follows.

Choosing a Lyapunov function candidate as $V_1 = s^2/2$ and computing the derivative of $\dot{V}_1$ along the system (16), it is obtained that

$$\begin{aligned} \dot{V}_1 = s\dot{s} = {} & c_2\left(d_2 - \hat{d}_2\right)s + c_3\left(d_3 - \hat{d}_3\right)s + \left(d_4 - \hat{d}_4\right)s + \dot{\tilde{d}}_2s \\ & + c_3\left(\dot{\tilde{d}}_2 - \dot{\hat{d}}_2\right)s + \dot{\tilde{d}}_3s - ks^2 - \varepsilon|s|. \end{aligned} \tag{31}$$

According to (26), (27), and (28), the following inequality is obtained as

$$\begin{aligned} \dot{V}_1 = {} & (c_2 + l_{22} + c_3l_{21})\tilde{d}_2s + (c_3 + l_{31})\tilde{d}_3s + \tilde{d}_4s - ks^2 - \varepsilon|s_h| \\ & \le -ks^2 - (\varepsilon - \eta)|s|. \end{aligned} \tag{32}$$

It is also obtained from (32) that system signals in system (16) can reach the sliding mode manifolds in finite time due to Lyapunov theory; that is, $s = 0$.

It is obtained that $x_4 = -c_1x_1 - c_2x_2 - c_3x_3 - \dot{\hat{d}}_2 - c_3\hat{d}_2 - \hat{d}_3$ when $s = 0$, and the system dynamic in the sliding mode will be governed as

$$\dot{x}_1 = x_2, \tag{33}$$

$$\dot{x}_2 = x_3 + d_2, \tag{34}$$

$$\dot{x}_3 = -c_1x_1 - c_2x_2 - c_3x_3 - \dot{\hat{d}}_2 - c_3\hat{d}_2 - \hat{d}_3 + d_3. \tag{35}$$

A corresponding Lyapunov function candidate is chosen as

$$V_2 = \mathbf{x}^T\mathbf{T}\mathbf{x}, \tag{36}$$

where $\mathbf{x} = [x_1\ x_2\ x_3 + d_2]^T$ and $\mathbf{T}$ is a positive matrix such that

$$\mathbf{A}^T\mathbf{T} + \mathbf{T}\mathbf{A} = -\mathbf{Q}, \tag{37}$$

for any given positive defined matrix $\mathbf{Q}$, where

$$\mathbf{T} = \begin{bmatrix} T_{11} & T_{12} & T_{13} \\ T_{12} & T_{22} & T_{23} \\ T_{13} & T_{23} & T_{33} \end{bmatrix}, \tag{38}$$

$$\mathbf{A} = \begin{bmatrix} 0 & 1 & 0 \\ 0 & 0 & 1 \\ -c_1 & -c_2 & -c_3 \end{bmatrix}, \tag{39}$$

are stable matrices. It is easily obtained that $\mathbf{T}$ is satisfied as the following conditions:

$$T_{11} = T_{13}c_2 + T_{23}c_1, \tag{40}$$

$$T_{12} = \frac{-q_2 + 2T_{23}c_2}{2} = T_{13}c_3 + T_{33}c_1, \tag{41}$$

$$T_{13} = \frac{q_1}{2c_1}, \tag{42}$$

$$T_{22} = -T_{13} + T_{23}c_3 + T_{33}c_2, \tag{43}$$

$$T_{23} = \frac{-q_3 + 2T_{33}c_3}{2}, \tag{44}$$

when $\mathbf{Q} = \operatorname{diag}(q_1, q_2, q_3)$, where $q_1 > 0$, $q_2 > 0$, and $q_3 > 0$.

Differentiating $\dot{V}_2$ along (33), (34), and (35) is

$$\begin{aligned}\dot{V}_2 = &-2T_{13}c_1x_1^2 + (2T_{12} - 2T_{23}c_2)x_2^2 \\ &+ (2T_{23} - 2T_{33}c_3)(x_3 + d_2)^2 \\ &+ (2T_{11} - 2T_{13}c_2 - 2T_{23}c_1)x_{1h}x_{2h} \\ &+ (2T_{12} - 2T_{13}c_3 - 2T_{33}c_1)x_1(x_3 + d_2) \\ &+ (2T_{13} + 2T_{22} - 2T_{23}c_3 - 2T_{33}c_2)x_{2h}(x_3 + d_{2h}) \\ &+ 2T_{13}x_1\left(c_3\tilde{d}_2 + \tilde{d}_3 + \dot{\tilde{d}}_2\right) + 2T_{23}x_2\left(c_3\tilde{d}_2 + \tilde{d}_3 + \dot{\tilde{d}}_2\right) \\ &+ 2T_{33}(x_3 + d_2)\left(c_3\tilde{d}_2 + \tilde{d}_3 + \dot{\tilde{d}}_2\right).\end{aligned} \tag{45}$$

Due to (37), it can be obtained as

$$\begin{aligned}\dot{V}_2 = &-q_1x_1^2 - q_2x_2^2 - q_3(e_3 + d_2)^2 + 2T_{13}x_1\left(c_3\tilde{d}_2 + \tilde{d}_3 + \dot{\tilde{d}}_2\right) \\ &+ 2T_{23}x_2\left(c_3\tilde{d}_2 + \tilde{d}_3 + \dot{\tilde{d}}_2\right) + 2T_{33}(x_3 + d_2)\left(c_3\tilde{d}_2 + \tilde{d}_3 + \dot{\tilde{d}}_2\right) \\ \le &-|x_1|(q_1|x_1| - 2T_{13}\mu) - |x_2|(q_2|x_2| - 2T_{23}\mu) \\ &- |x_3 + d_2|(q_3|x_3 + d_2| - 2T_{33}\mu),\end{aligned} \tag{46}$$

where $\mu = |c_3\tilde{d}_2 + \tilde{d}_3 + \dot{\tilde{d}}_2|$. It is easily obtained from (46) that

$$\mu \le (c_3 + 1)\lambda_2 + \lambda_3. \tag{47}$$

From inequality (47), the error states of the velocity subsystem are bounded, that is,

$$|x_1| \le \frac{2T_{13}\mu}{q_1}, \tag{48}$$

$$|x_2| \le \frac{2T_{23}\mu}{q_2}, \tag{49}$$

$$|x_3 + d_2| \le \frac{2T_{33}\mu}{q_3}. \tag{50}$$

Remark 2. It is worth noting that the state x_1 can be reduced by increasing q_1 or decreasing λ_j $(j = 2, 3)$ according to (47), (48), (49), and (50). With increasing q_1, the T_{13} increases due to (40), (41), (42), (43), and (44). Only when the estimate accuracy of d_j $(j = 2, 3)$ is improved by the nonlinear disturbance observers (17), (18), (19), (20), (21), (22), (23), and (24) can λ_j be reduced and the accuracy of the state x_1 be also increased. In fact, the impact of the LOS angle error is satisfied with $|e_q| \le 2T_{13}\mu/q_1$ due to the definition of the state x_1; that is, it is obtained from the relationship between the accuracy of the LOS angle error and the estimate error of nonlinear disturbances. In other words, it is obtained from the relationship between the accuracy of impact angle and the estimate errors of nonlinear disturbances from (48), (49), and (50).

4. Simulation

In this section, the effectiveness of the proposed IGC law is verified by the nonlinear numerical simulations. For the nonlinear numerical simulations, the original nonlinear motion model of the missile given in [23] and the relative motion model between the missile and target given in [25] are adopted, and the aerodynamic forces, moments, and nominal parameters are obtained in [4].

The simulation step is 0.001 s; the initial values of the simulation are assumed to be $q_M = -90$ deg, $V_M = 200$ m/s, $\alpha(0) = 0$ deg, $\omega_z(0) = 0$ rad/s, and $R(0) = 3000$ m. Parameters of the proposed IGC law are $c_1 = 9$, $c_2 = 11$, $c_3 = 8$, $k = 0.975$, and $\varepsilon = 0.2$.

In addition, the uncertainties of missile-related aerodynamic parameters can include 20% variations with respect to their normal values; some requirements for the guidance and control system are listed as follows:

(1) The blind area for the homing guidance seeker is 50 m.

(2) The miss distance is no more than 0.5 m.

(3) The absolute error of terminal impact angle distance is no more than 5 deg.

(4) The angle of attack is less than 10 deg.

(5) The fin deflection limit and fin rate limit are restricted as $|\delta| \le 10$ deg and $|\dot{\delta}| \le 100$ deg/s.

(6) The states of the missile are bounded.

For comparison studies, two control laws are introduced to the nonlinear numerical simulations. The first is the classical guidance and control (CGC) law [1], which treats the guidance and control system as two separate processes, and the second is the partial integrated guidance and control (PIGC) law [11], which combines the backstepping technique and sliding mode control method.

In order to demonstrate the performance of the proposed IGC law in the presence of uncertainties in the parameters, three cases are considered for a homing missile against a fixed target, a moving target, and a maneuvering target on the ground.

Case 1. Variable response curves of the guidance and control system under the three control laws against a fixed target on the ground are shown in Figure 2. The estimate errors of disturbances coming from the nonlinear disturbance observer are shown in Figure 3. Missile/target trajectories under the three control laws are shown in Figure 4(a). Miss distance and impact angle under the three control laws are shown in Tables 1 and 2, respectively.

As presented in Figure 2, the LOS angle rate under the CGC law slowly converges to zero in the terminal phase, while the LOS angle rate under the IGC law rapidly converges to zero in Figure 2(a). Meanwhile, the angle of attack, pitch rate, and elevator deflection under the PIGC law vary more acutely than the other laws at two seconds from

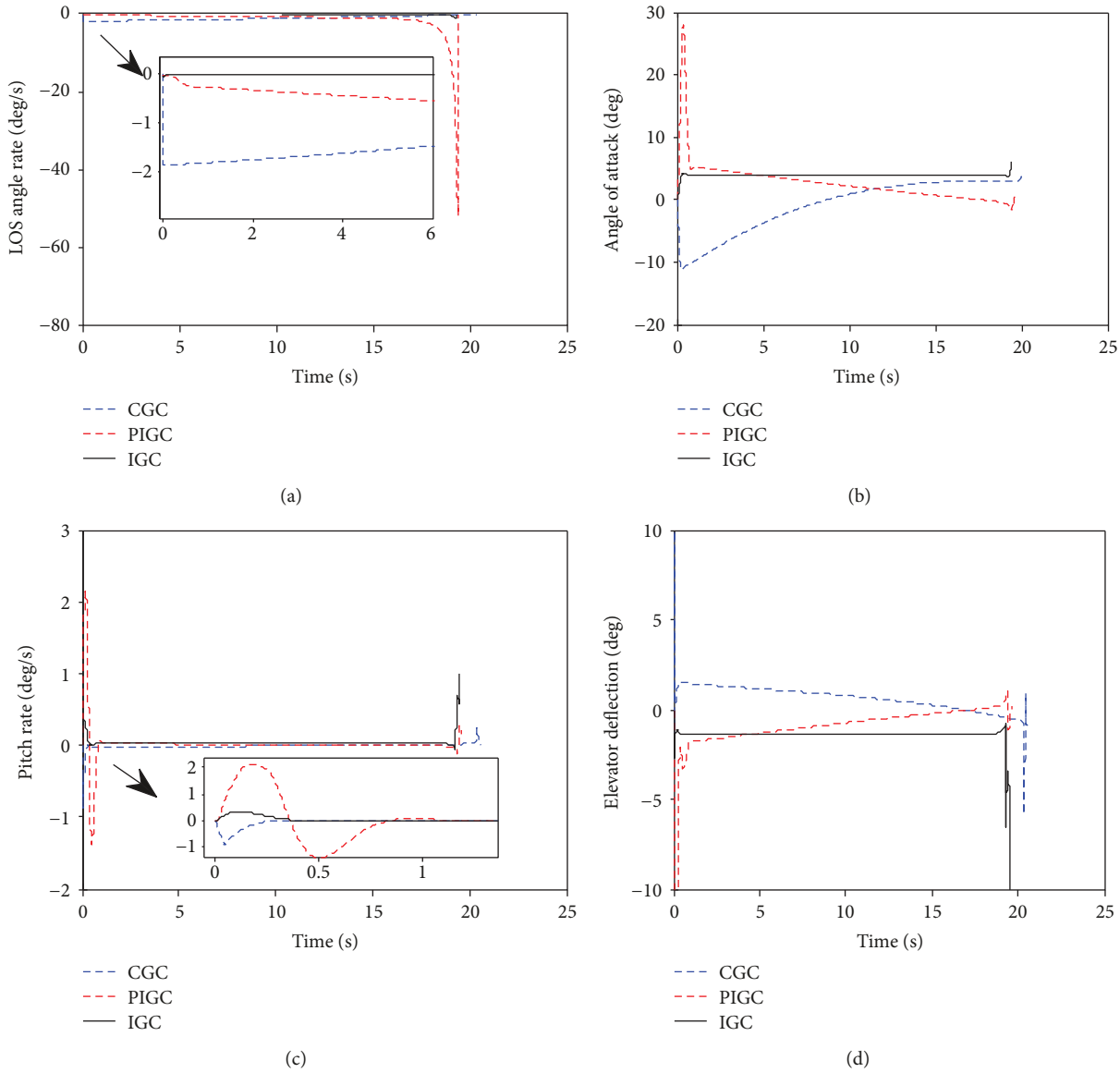

Figure 2: Variable response curves under the three control laws against a fixed target.

Figures 2(b)–2(d), and the angle of attack is more than 10 deg under the PIGC law. Even when the target enters the homing head blind zone, the elevator deflection still works under the IGC law as shown as Figure 2(d). The states have been stabilized more rapidly under the IGC law than the other control laws because the disturbance observer technique is employed to estimate the unknown uncertainties, and the estimate errors quickly converge to zero under the designed nonlinear disturbance observer as shown in Figure 3. Both miss distance and impact angle under the IGC law achieve the satisfactory performance.

Moreover, the time under the IGC law is about 0.1 s shorter than that of the PIGC law and about 0.6 s shorter than that of the CGC law against a fixed target on the ground.

Case 2. To make the work more challenging, the target moves at 20 m/s on the ground in this case. Missile/target trajectories under the three control laws are shown in Figure 4(b), and variable response curves of the missile guidance and control system under the three control laws against a moving target are shown in Figure 5. Miss distance and impact angle under the three control laws are shown in Tables 3 and 4, respectively.

From the simulation results among the three control laws, the states are stabilized most rapidly under the IGC; both miss distance and impact angle under the IGC law also achieve satisfactory performance. The time in the simulation experiment under the IGC law is about 0.1 s shorter than that of the PIGC law and about 0.5 s shorter than that of the CGC law against a moving target on the ground.

Case 3. In this case, the target on the ground moves with a maneuver of $2.4\cos(0.1t)$ m/s; the variable response curves of the missile guidance and control system under the three control laws are shown in Figure 6. Miss distance and impact angle under the three control laws are

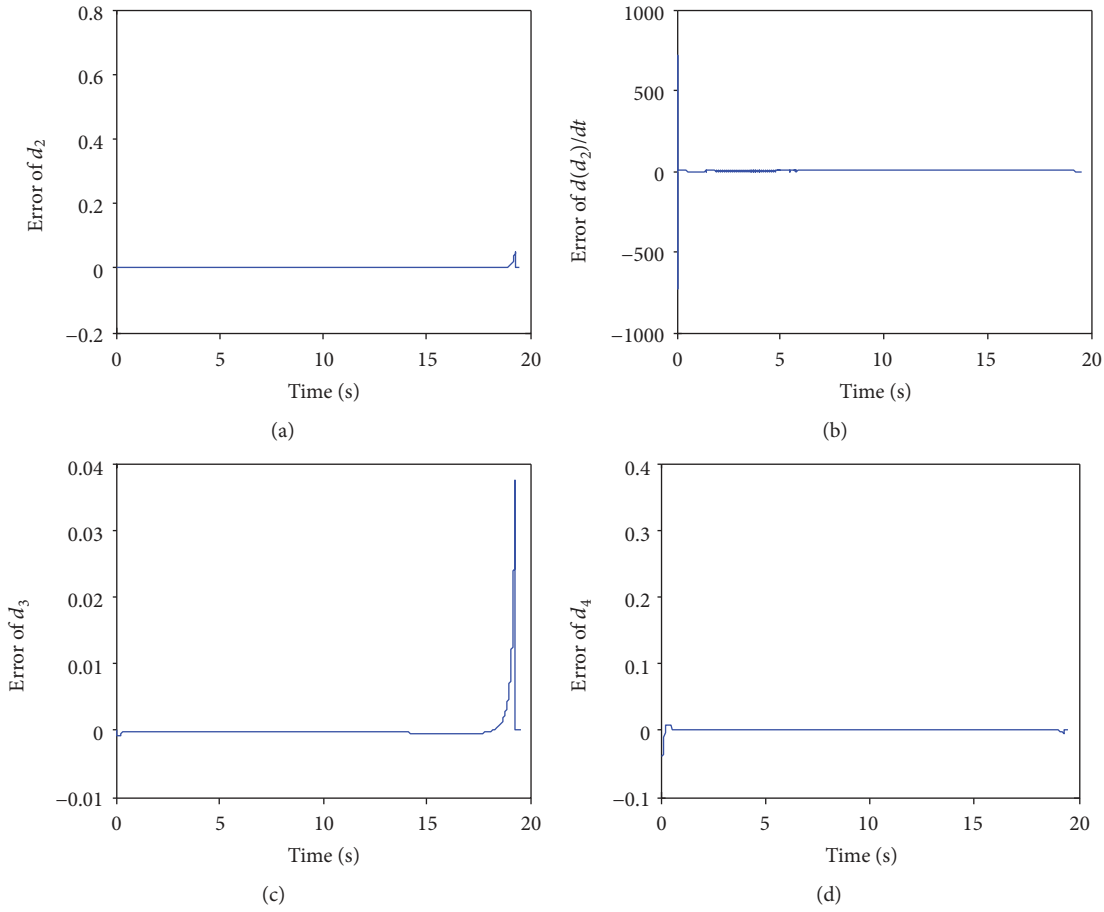

Figure 3: Estimate curves of uncertainties under the nonlinear disturbance observer.

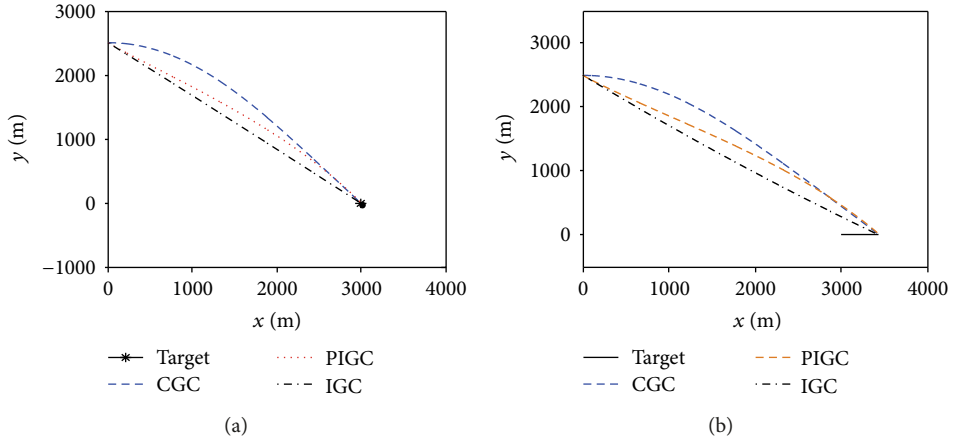

Figure 4: Missile/target trajectories under the three control laws against a fixed target and a moving target.

Table 1: Miss distance under the three control laws against a fixed target.

CGC law	PIGC law	IGC law
0.09943 m	5.611 m	0.2059 m

Table 2: Impact angle under the three control laws against a fixed target.

CGC law	PIGC law	IGC law
−62.8 deg	−89.7 deg	−88.7 deg

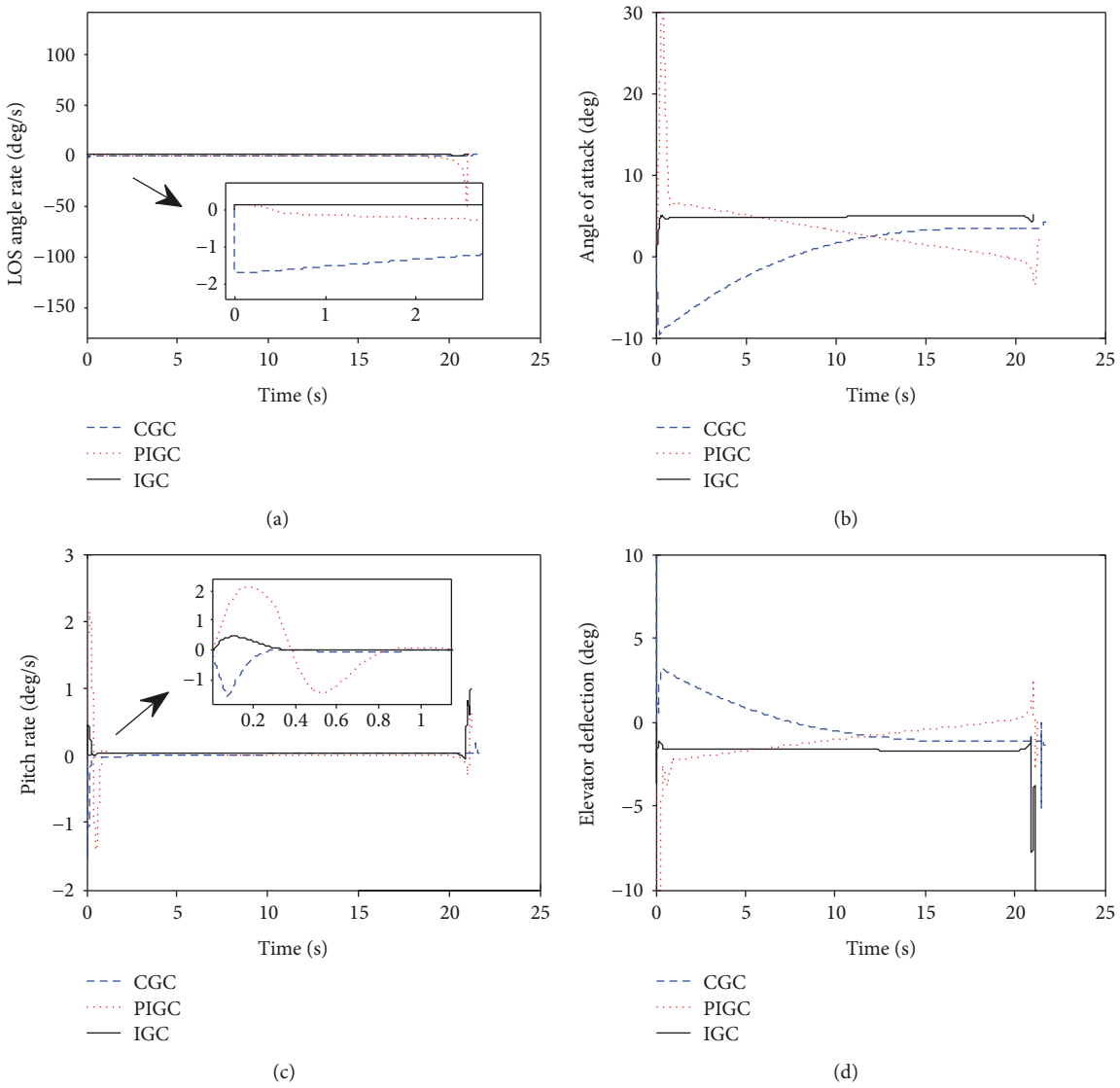

Figure 5: Variable response curves under the three control laws against a moving target.

Table 3: Miss distance under the three control laws against a moving target.

CGC law	PIGC law	IGC law
0.093 m	11.4 m	0.4426 m

Table 4: Impact angle under the three control laws against a moving target.

CGC law	PIGC law	IGC law
−68.1 deg	−89.9 deg	−86.2 deg

also shown in Tables 5 and 6, respectively. The same results can be also obtained from the simulation results. The time in the simulation experiment under the IGC law is about 0.1 s shorter than that of the PIGC law, and it is about 1.4 s shorter than that of the CGC law against a maneuvering target.

In short, it is easily obtained that the states are stabilized most rapidly; both the miss distance and the impact angle can be satisfied under the IGC law, while only partial index can be satisfied under the CGC law and the PIGC law. Meanwhile, the flight time of engagement with a fixed target, a moving target, and a maneuvering target is shortened by utilizing the proposed IGC law, compared with the CGC law and the PIGC law.

5. Conclusion

A novel IGC law for a homing missile with impact angle constraint is proposed against a ground target to improve the rapidity of the missile guidance and control system. A new control-oriented model with impact angle error of the IGC system in the pitch plane is built, and an IGC law is

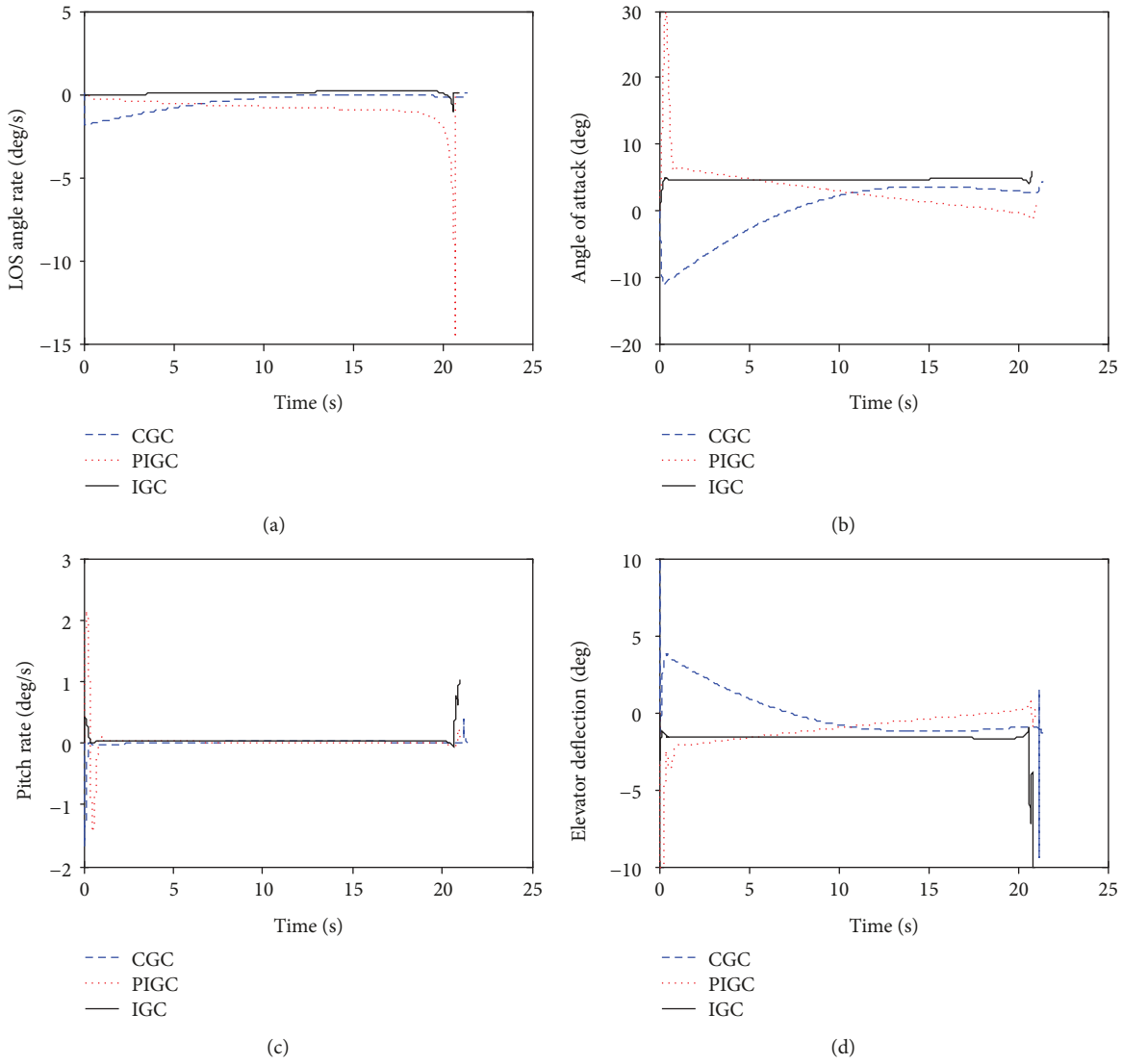

Figure 6: Variable response curves under the three control laws against a maneuvering target.

Table 5: Miss distance under the three control laws against a maneuvering target.

CGC law	PIGC law	IGC law
0.067 m	3.176 m	0.4221 m

Table 6: Impact angle under the three control laws against a maneuvering target.

CGC law	PIGC law	IGC law
−67.6 deg	−89.4 deg	−84.9 deg

designed by utilizing the sliding mode control and the nonlinear disturbance observer. The relationship between the accuracy of impact angle and the estimate error of mismatched uncertainties can be obtained from the stability of the system. Simulation results have shown that the proposed IGC approach achieves good performance and shortens the time of engagement.

Data Availability

The data used to support the findings of this study are available from the corresponding author upon request.

Conflicts of Interest

The authors declare that they have no conflicts of interest.

Acknowledgments

This work is supported by the National Nature Science Foundation of China under Grant 61703339.

References

[1] M. Levy, T. Shima, and S. Gutman, "Linear quadratic integrated versus separated autopilot-guidance design," *Journal of Guidance, Control, and Dynamics*, vol. 36, no. 6, pp. 1722–1730, 2013.

[2] P. K. Menon and E. J. Ohlmeyer, "Integrated design of agile missile guidance and autopilot systems," *Control Engineering Practice*, vol. 9, no. 10, pp. 1095–1106, 2001.

[3] N. F. Palumbo, B. E. Reardon, and R. A. Blauwkamp, "Integrated guidance and control for homing missiles," *Johns Hopkins APL Technical Digest*, vol. 25, no. 2, pp. 121–139, 2004.

[4] M. Z. Hou, X. L. Liang, and G. R. Duan, "Adaptive block dynamic surface control for integrated missile guidance and autopilot," *Chinese Journal of Aeronautics*, vol. 26, no. 3, pp. 741–750, 2013.

[5] D. E. Williams, J. Richman, and B. Friedland, "Design of an integrated strapdown guidance and control system for a tactical missile," in *Guidance and Control Conference*, pp. 57–66, Gatlinburg, TN, USA, August 1983.

[6] T. Shima, M. Idan, and O. M. Golan, "Sliding mode control for integrated missile autopilot-guidance," in *AIAA Guidance, Navigation, and Control Conference and Exhibit*, Providence, Rhode Island, August 2004.

[7] D. Chwa, J. Y. Choi, and S. G. Anavatti, "Observer-based adaptive guidance law considering target uncertainties and control loop dynamics," *IEEE Transactions on Control Systems Technology*, vol. 14, no. 1, pp. 112–123, 2006.

[8] M. Xin, S. N. Balakrishnan, and E. J. Ohlmeyer, "Integrated guidance and control of missiles with θ-D method," *IEEE Transactions on Control Systems Technology*, vol. 14, no. 6, pp. 981–992, 2006.

[9] R. Padhi and C. Chawla, "Neuro-adaptive augmented dynamic inversion based PIGC design for reactive obstacle avoidance of UAVs," in *AIAA Guidance, Navigation, and Control Conference*, Portland, Oregon, August 2011.

[10] X. Wang and J. Wang, "Partial integrated guidance and control for missiles with three-dimensional impact angle constraints," *Journal of Guidance, Control, and Dynamics*, vol. 37, no. 2, pp. 644–657, 2014.

[11] X. Wang and J. Wang, "Partial integrated guidance and control with impact angle constraints," *Journal of Guidance, Control, and Dynamics*, vol. 38, no. 5, pp. 925–936, 2015.

[12] F. B. Ibarrondo and P. Sanz-Aránguez, "Integrated versus two-loop guidance-autopilot for a dual control missile with high-order aerodynamic model," *Proceedings of the Institution of Mechanical Engineers, Part G: Journal of Aerospace Engineering*, vol. 230, no. 1, pp. 60–76, 2016.

[13] X. Liu, W. Huang, and L. du, "An integrated guidance and control approach in three-dimensional space for hypersonic missile constrained by impact angles," *ISA Transactions*, vol. 66, pp. 164–175, 2017.

[14] H. Yan, S. P. Tan, and Y. Z. He, "A small-gain method for integrated guidance and control in terminal phase of reentry," *Acta Astronautica*, vol. 132, pp. 282–292, 2017.

[15] H. Yan, X. Wang, B. Yu, and H. Ji, "Adaptive integrated guidance and control based on backstepping and input-to-state stability," *Asian Journal of Control*, vol. 16, no. 2, pp. 602–608, 2014.

[16] S. Wang, W. H. Wang, and S. F. Xiong, "Impact angle constrained three-dimensional integrated guidance and control for STT missile in the presence of input saturation," *ISA Transactions*, vol. 64, pp. 151–160, 2016.

[17] H. Song and T. Zhang, "Fast robust integrated guidance and control design of interceptors," *IEEE Transactions on Control Systems Technology*, vol. 24, no. 1, pp. 349–356, 2016.

[18] Z. Cong and W. Yun-jie, "Non-singular terminal dynamic surface control based integrated guidance and control design and simulation," *ISA Transactions*, vol. 63, pp. 112–120, 2016.

[19] S. He, T. Song, and D. Lin, "Impact angle constrained integrated guidance and control for maneuvering target interception," *Journal of Guidance, Control, and Dynamics*, vol. 40, no. 10, pp. 2653–2661, 2017.

[20] S. M. He, J. Wang, and W. Wang, "A novel sliding mode guidance law without line-of-sight angular rate information accounting for autopilot lag," *International Journal of Systems Science*, vol. 48, no. 16, pp. 3363–3373, 2017.

[21] J. G. Guo, Y. Xiong, and J. Zhou, "A new sliding mode control design for integrated missile guidance and control system," *Aerospace Science and Technology*, vol. 78, pp. 54–61, 2018.

[22] H. Mingzhe and D. Guangren, "Integrated guidance and control of homing missiles against ground fixed targets," *Chinese Journal of Aeronautics*, vol. 21, no. 2, pp. 162–168, 2008.

[23] X. F. Qian, R. X. Lin, and Y. N. Zhao, *Missile Flight Mechanics*, Beijing Institute of Technology Press, Beijing, 2000.

[24] D. Ginoya, P. D. Shendge, and S. B. Phadke, "Sliding mode control for mismatched uncertain systems using an extended disturbance observer," *IEEE Transactions on Industrial Electronics*, vol. 61, no. 4, pp. 1983–1992, 2014.

[25] D. Zhou, C. D. Mu, and W. L. Xu, "Adaptive sliding-mode guidance of a homing missile," *Journal of Guidance, Control, and Dynamics*, vol. 22, no. 4, pp. 589–594, 1999.